J Supercond Nov Magn (2011) 24:1985–1989
DOI 10.1007/s10948-011-1157-x

ORIGINAL PAPER

Improvement of Superconductivity with the Modification of Charge Reservoir Layer in $(Cu_{0.5}Tl_{0.5-x}M_x)Ba_2Ca_2Cu_3O_{10-\delta}$

M. Mumtaz · Nawazish A. Khan · Faheem Ashraf

Received: 13 February 2011 / Accepted: 2 March 2011 / Published online: 23 March 2011

Abstract The relatively higher electronegative elements (M = Pd, Nb, Bi, Hg) have been partially doped at Tl sites in $Cu_{0.5}Tl_{0.5-x}M_xBa_2O_{4-\delta}$ ($x = 0, 0.25$) charge reservoir layer of $Cu_{0.5}Tl_{0.5-x}M_xBa_2Ca_2Cu_3O_{10-\delta}$ superconductor. These elements may retain more oxygen in the charge reservoir layer due to their higher electronegativity as compared to Tl, and the higher population of oxygen in the charge reservoir layer can optimize the charge carriers' density in the conducting CuO_2 planes. The optimum density of mobile charge carriers in the conducting CuO_2 increases Fermi wave-vector K_F and Fermi velocity υ_F of the carriers, which results in the improvement of superconducting properties of the material.

Keywords $Cu_{0.5}Tl_{0.5-x}M_xBa_2Ca_2Cu_3O_{10-\delta}$ superconductor · Electronegative · Doping · Charge reservoir layer

1 Introduction

There are two major parts of the unit cell of all the cuprate high-temperature superconductors (HTSCs) [1];

(1) An $MBa_2O_{4-\delta}$ charge reservoir layer (M = Cu, Tl, Hg, Bi, C, etc.).
(2) Conducting $nCuO_2$ planes ($n = 2, 3, 4, 5, 6$).

M. Mumtaz (✉) · N.A. Khan · F. Ashraf
Materials Science Laboratory, Department of Physics, Quaid-i-Azam University, Islamabad 45320, Pakistan
e-mail: mmumtaz75@yahoo.com

M. Mumtaz
Department of Physics, FBAS, International Islamic University (IIU), Islamabad 44000, Pakistan

The charge reservoir layer supplies the charge carriers to conducting CuO_2 planes, where the superconductivity was supposed to be taken place [2–5]. The number of the carriers supplied to the conducting CuO_2 planes critically depends on the composition of charge reservoir layers; therefore, the study of the composition of charge reservoir in high-T_c superconductivity is of special significance. The composition of the charge reservoir layer can be modified by the doping of selective elements such as Co, Fe, Al, Cu, Tl, Hg, Bi, C, etc. in $MBa_2O_{4-\delta}$ a charge reservoir layer [6–13]. The appropriate ratio of elements at the charge reservoir layer can optimally dope the conducting CuO_2 planes with charge carriers. The optimum carriers density in the conducting planes fixes the Fermi wave-vector ($K_F = (3\pi^2 \frac{N}{V})^{1/3}$, which is related to the coherence length ($\xi_c = \frac{\hbar K_F}{2m\Delta}$) and Fermi velocity ($\upsilon_F = \frac{\pi \xi_c \Delta}{\hbar}$) of the carriers; Δ is pairing potential [14, 15]. The increased υ_F along c-axis can enhance the transport properties [i.e., critical temperature (T_c), current density (J_c)] and magnitude of diamagnetism of the final compound. In our continued research on CuTl-based HTSCs family, we have observed that superconducting properties (higher T_c, magnitude of diamagnetism and J_c) can be improved by decreasing anisotropy of the final compound. This was achieved by Mg and Be doping at Ca sites in CuTl-based HTSCs. The doping of these elements has improved interplane coupling by decreasing c-axis length of the unit cell of the final compound [16, 17]. In the present article, we have presented the effects of modified structure of the charge reservoir layer in $(Cu_{0.5}Tl_{0.5-x}M_x)Ba_2Ca_2Cu_3O_{10-\delta}$ superconductor by the partial doping of relatively higher electronegative (M = Pd, Nb, Bi, Hg) elements as compared to Tl at Tl sites in $(Cu_{0.5}Tl_{0.5-x}M_x)Ba_2O_{4-\delta}$ charge reservoir layer.

2 Experimental

The ceramic superconducting $(Cu_{0.5}Tl_{0.5-x}M_x)Ba_2Ca_2Cu_3O_{10-\delta}$; (M = Pd, Nb, Bi, Hg, $x = 0$, 0.25) material was synthesized by the solid-state reaction method in two steps. In the first step, different compounds such as $Cu_2(CN)_2$, $Ba(NO_3)_2$ and $CaCO_3$ were mixed according to the required composition and ground for about an hour in a quartz mortar and pestle. These ground materials were loaded in a quartz boat and fired at 840 °C for 24 hours in preheated chamber furnace and then cooled to the room temperature. The fired $Cu_{0.5}Ba_2Ca_2Cu_3O_{10-\delta}$ precursor material was mixed with the appropriate ratio of Tl_2O_3, $PdCl_2$, Nb_2O_5, Bi_2O_3, and Hg_2O_3 and ground again for about an hour. The ground material once again was loaded in a quartz boat and fired at 840 °C for 24 hours and then cooled to the room temperature to get $(Cu_{0.5}Tl_{0.5-x}M_x)Ba_2Ca_2Cu_3O_{10-\delta}$ as final reactant composition. The final reactant composition of $(Cu_{0.5}Tl_{0.5-x}M_x)Ba_2Ca_2Cu_3O_{10-\delta}$ material was pelletized under 3.5 tons/cm^2 pressure and the pellets were enclosed in gold capsules and heat-treated at temperature 840 °C for 10 minutes. After 10 minutes heat-treatment, the pellets in gold capsules were quenched to room temperature.

The structural properties of the material were determined by X-ray diffraction (XRD) and the physical properties such as resistivity by four-probe method and bulk superconductivity by ac-susceptibility measurements with mutual induction method. The phonon modes associated with the vibrations of oxygen atoms were measured by Fourier Transform Infrared (FTIR) spectroscopy.

3 Results and Discussion

The X-ray diffraction (XRD) scans of $(Cu_{0.5}Tl_{0.5-x}M_x)Ba_2Ca_2Cu_3O_{10-\delta}[Cu_{0.5}Tl_{0.5-x}M_x\text{-}1223]$ samples doped with relatively higher electronegative elements such as M = Pd, Nb, Bi, Hg are shown in Fig. 1. Most of the diffraction peaks in these XRD scans are indexed according to tetragonal P4/mmm space group and the cell parameters calculated after fitting these peaks are given along with each diffractogram. The relative percentages of the derivative phases present in the material are calculated as:

$$\text{CuTl-1223}(\%) = \frac{\sum I(\text{CuTl-1223})}{\sum I(\text{CuTl-1223}) + \sum I(\text{CuTl-1234}) + \sum I(\text{CuTl-1212})} \times 100$$

$$\text{CuTl-1234}(\%) = \frac{\sum I(\text{CuTl-1234})}{\sum I(\text{CuTl-1223}) + \sum I(\text{CuTl-1234}) + \sum I(\text{CuTl-1212})} \times 100$$

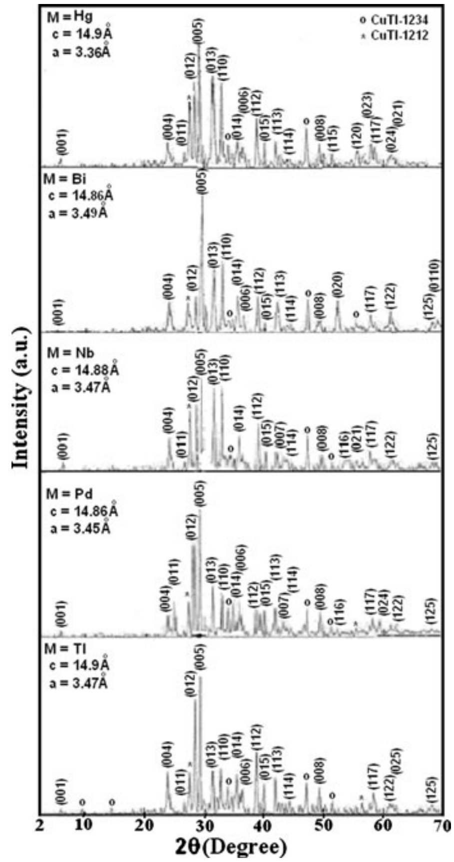

Fig. 1 The XRD patterns of $Cu_{0.5}Tl_{0.5-x}M_xBa_2Ca_2Cu_3O_{10-\delta}$ (M = 0, Pd, Nb, Bi, Hg) superconductor samples

$$\text{CuTl-1212}(\%) = \frac{\sum I(\text{CuTl-1212})}{\sum I(\text{CuTl-1223}) + \sum I(\text{CuTl-1234}) + \sum I(\text{CuTl-1212})} \times 100$$

where I is the intensity of the different phases present in the samples [18]. The percentages of the different phases present in the samples calculated using the above expressions are given in Table 1.

The resistivity measurements of $Cu_{0.5}Tl_{0.5-x}M_x$-1223 samples doped with M = Pd, Nb, Bi, Hg at Tl sites in $Cu_{0.5}Tl_{0.5-x}M_xBa_2O_{4-\delta}$ charge reservoir layer are shown in Fig. 2. These samples have metallic variation of resistivity from room temperature down to onset of superconductivity. The comparison showed that the normal state resistivity has been increased with Pd and Nb substitution and it has been decreased with Bi and Hg substitution. The undoped $(Cu_{0.5}Tl_{0.5})Ba_2Ca_2Cu_3O_{10-\delta}$ superconductor has shown zero-resistivity critical temperature $[T_c(R = 0)]$ at 95 K, which has been increased to 105, 104, 98, 106 K with the partial doping of M = Pd, Nb, Bi, Hg, respectively. The ac-susceptibility measurements of $Cu_{0.50}Tl_{0.5-x}M_x$-1223 samples are shown in Fig. 3. In

Table 1 Volume fractions of the various phases present in $Cu_{0.5}Tl_{0.5-x}M_xBa_2Ca_2Cu_3O_{10-\delta}$ (M = 0, Pd, Nb, Bi, Hg) superconductor samples

Sr. No.	Concentration of dopants	% of CuTl-1223 phase	% of CuTl-1234 phase	% of CuTl-1212 phase
1	M = 0, Tl = 0.5	84	11	5
2	M = Pd = 0.25, Tl = 0.25	85	10	5
3	M = Nb = 0.25, Tl = 0.25	82	9	9
4	M = Bi = 0.25, Tl = 0.25	83	11	6
5	M = Hg = 0.25, Tl = 0.25	84	4	12

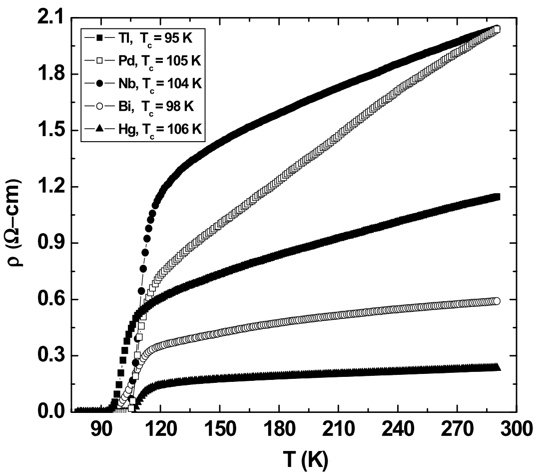

Fig. 2 The resistivity vs. temperature measurements of $Cu_{0.5}Tl_{0.5-x}M_xBa_2Ca_2Cu_3O_{10-\delta}$ (M = 0, Pd, Nb, Bi, Hg) superconductor samples

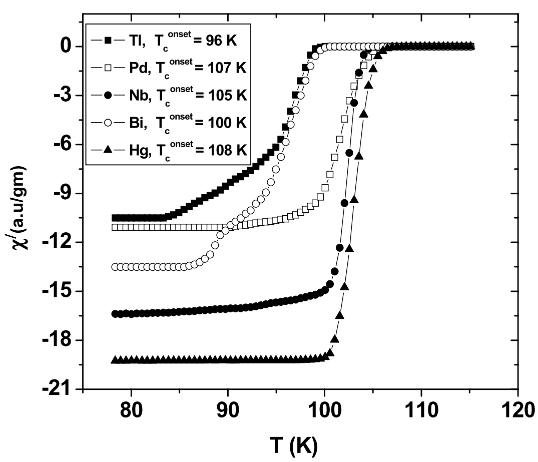

Fig. 3 The ac-susceptibility vs. temperature measurements of $Cu_{0.5}Tl_{0.5-x}M_xBa_2Ca_2Cu_3O_{10-\delta}$ (M = 0, Pd, Nb, Bi, Hg) superconductor samples

the undoped $(Cu_{0.5}Tl_{0.5})Ba_2Ca_2Cu_3O_{10-\delta}$ samples the onset of diamagnetism is at 96 K, which has been shifted to higher values of 107, 105, 100, 108 K with the doping of M = Pd, Nb, Bi, Hg, respectively. The relative magnitude of diamagnetism has been increased with the partial substitution of relatively higher electronegative elements

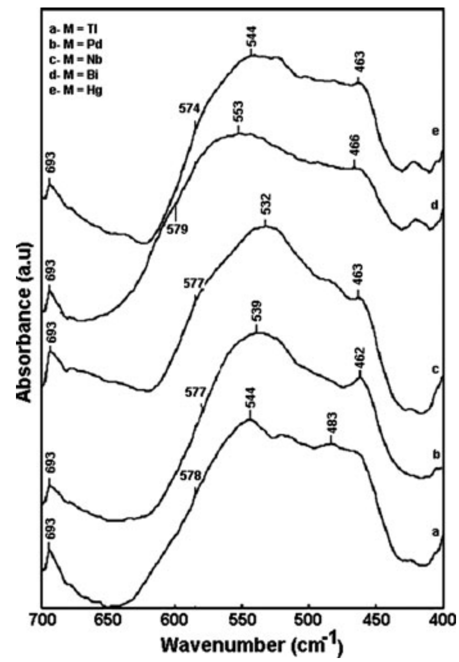

Fig. 4 The FTIR absorption spectra of $Cu_{0.5}Tl_{0.5-x}M_xBa_2Ca_2Cu_3O_{10-\delta}$ (M = 0, Pd, Nb, Bi, Hg) superconductor samples

at Tl sites in charge reservoir layer as compared to the undoped samples. The doped elements M = Pd, Nb, Bi, Hg with relatively higher electronegativity retain more oxygen in the $Cu_{0.5}Tl_{0.5-x}M_xBa_2O_{4-\delta}$ charge reservoir layer, which tends to optimize the hole density in the CuO_2 planes. Therefore, the superconducting properties have been improved with the doping of these elements.

Since the concentration of charge carriers in the conducting CuO_2 planes is modified by changing the structure of $Cu_{0.5}Tl_{0.5-x}M_xBa_2O_{4-\delta}$ charge reservoir layer with the partial substitution of M = Pd, Nb, Bi, Hg at Tl sites, it may change the vibrational frequencies of oxygen-related phonon modes in $Cu_{0.5}Tl_{0.5-x}M_xBa_2Ca_2Cu_3O_{10-\delta}$ superconductor. These effects have been investigated by FTIR absorption measurements in the wavenumber range of 400 to 700 cm^{-1}, Fig. 4. The oxygen-related phonon modes in $Cu_{0.5}Tl_{0.5}Ba_2Ca_2Cu_3O_{10-\delta}$ superconductor have been observed around 483, 544, 578, 693 cm^{-1} and these modes correspond to the apical oxygen of types Tl-O_A-Cu(2) and

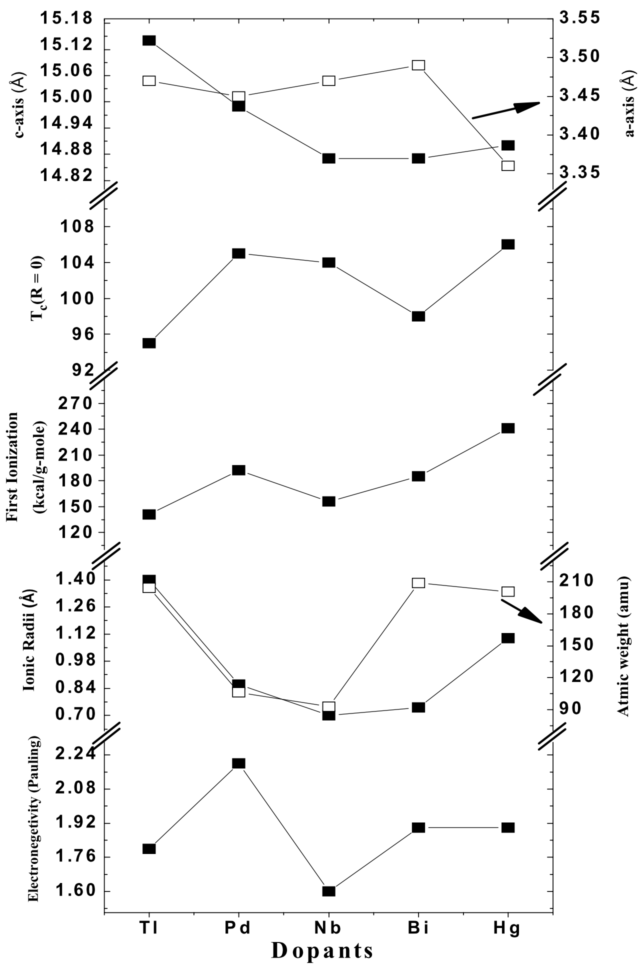

Fig. 5 The comparison of electronegativity, ionic radii, atomic weight and first ionization of doped elements (i.e., 0, Pd, Nb, Bi, Hg) and $T_c(R = 0)$, c-axis and a-axis of $Cu_{0.5}Tl_{0.5-x}M_xBa_2Ca_2Cu_3O_{10-\delta}$ (M = 0, Pd, Nb, Bi, Hg) superconductor samples

Cu(1)-O_A-Cu(2), planar oxygen Cu(2)-O_P-Cu(2) and O3 atoms in $Cu_{0.5}Tl_{0.5}Ba_2O_{4-\delta}$ charge reservoir layer [19]. These modes in Pd-doped $Cu_{0.5}Tl_{0.5-x}Pd_xBa_2Ca_2Cu_3O_{10-\delta}$ superconductor are observed at 462, 539, 577, 693 cm^{-1} and in Nb-doped $Cu_{0.5}Tl_{0.5-x}Nb_xBa_2Ca_2Cu_3O_{10-\delta}$ superconductor these modes are observed at 463, 532, 577, 693 cm^{-1}, respectively. These modes in Bi-doped $Cu_{0.5}Tl_{0.5-x}Bi_xBa_2Ca_2Cu_3O_{10-\delta}$ superconductor are observed at 466, 553, 579, 693 cm^{-1} and in Hg-doped $Cu_{0.5}Tl_{0.5-x}Hg_xBa_2Ca_2Cu_3O_{10-\delta}$ these modes are observed at 463, 544, 574, 693 cm^{-1}, respectively. In the Nb- and Pd-doped samples, the apical oxygen modes of type Cu(1)-O_A-Cu(2) have been softened from 544 cm^{-1} to 539 and 532 cm^{-1}, respectively, and have been hardened to 553 cm^{-1} with Bi-doping, but remain at the same position (~544 cm^{-1}) in Hg-doped samples. Moreover, the apical oxygen modes of type M-O_A-Cu(2) are also softened from 483 cm^{-1} to 462, 463, 466, 463 cm^{-1} in M = Pd, Nb, Bi, Hg-doped samples, respectively. These changes in oxygen-related phonon modes are most probably linked with different masses of the doped elements. The planar oxygen Cu(2)-O_P-Cu(2) modes and O3 modes almost remain fixed about 577 and 693 cm^{-1}, respectively, as shown in Fig. 4. The increased intensity of these modes is the indirect evidence of higher population of oxygen in $Cu_{0.5}Tl_{0.5-x}M_xBa_2O_{4-\delta}$ charge reservoir layer of the doped material. The higher electronegative elements possibly modify the carriers transfer mechanism from charge reservoir layer to conducting CuO_2 planes to attain the optimum level of carriers' density.

The relative comparison of electronegativity, ionic radii, atomic weight and first ionization of doped elements (i.e., M = Pd, Nb, Bi, Hg) with Tl and $T_c(R = 0)$, c-axis and a-axis of $Cu_{0.5}Tl_{0.5-x}M_xBa_2Ca_2Cu_3O_{10-\delta}$ superconductor samples are shown in Fig. 5. The ionic radii of the doped elements (M = Pd, Nb, Bi, Hg) are smaller than that of Tl and the c-axis length of $Cu_{0.5}Tl_{0.5-x}M_xBa_2Ca_2Cu_3O_{10-\delta}$ superconductor decreases with the partial doping of M = Pd, Nb, Bi, Hg elements at Tl sites. The three-dimensional (3D) conductivity has been improved in $Cu_{0.5}Tl_{0.5-x}M_xBa_2Ca_2Cu_3O_{10-\delta}$ superconductor with the decrease of c-axis length and hence the $T_c(R = 0)$ has been increased.

4 Conclusions

The ceramic superconducting $Cu_{0.5}Tl_{0.5-x}M_xBa_2Ca_2Cu_3O_{10-\delta}$ material with modified structure of $Cu_{0.5}Tl_{0.5-x}M_xBa_2O_{4-\delta}$ charge reservoir layer has been synthesized at normal pressure. The decreased c-axis length with the partial doping of M = Pd, Nb, Bi, Hg at Tl sites in $Cu_{0.5}Tl_{0.5-x}M_xBa_2Ca_2Cu_3O_{10-\delta}$ material has improved the 3D conductivity in the unit cell. It has been observed that the doping of relatively higher electronegative (M = Pd, Nb, Bi Hg) elements promotes the optimum carriers density in CuO_2 planes of $Cu_{0.5}Tl_{0.5-x}M_xBa_2Ca_2Cu_3O_{10-\delta}$ superconductor, which causes the enhanced superconductivity. Hence, modification of the charge reservoir layer can alter the superconducting properties of the material.

Acknowledgements Higher Education Commission (HEC) Pakistan through project No. 20-1482/R&D/09/1482 is acknowledged for their financial support.

References

1. Park, C., Synder, R.L.: J. Am. Ceram. Soc. **78**, 3171 (1995)
2. Mattheiss, L.F.: Phys. Rev. B **42**, 10108 (1990)
3. Karppinen, M., Yamauchi, H.: Philos. Mag., B **79**, 343 (1999)
4. Yamauchi, H., Karppinen, M.: J. Low Temp. Phys. **117**, 813 (1999)
5. Yamauchi, H., Karppinen, M., Morita, Y., Kitabatake, M., Motohashi, T., Liu, R.S., Lee, J.M., Chen, J.M.: J. Solid State Chem. **177**, 1037 (2004)

6. Abou-Aly, A.I., Awad, R., Mohammed, N.H.: J. Magn. Magn. Mater. **226–230**, 328 (2001)
7. Lai, C.C., Ho, P.C., Hung, C.Y., Ku, H.C., Lin, T.Y.: Chin. J. Phys. **29**, 57 (1991)
8. Awad, R., Shukor, A., Tee, K.S.: J. Mater. Sci. Lett. **17**, 103 (1998)
9. Shibata, T., Tatsuki, T., Adachi, S., Tanabe, K., Fujihara, S., Kimura, T.: Physica C **353**, 200 (2001)
10. Tokiwa, K., Kunugi, C., Kashwagi, H., Nibe, T., Ichioka, N., Watanabe, T., Iyo, A., Tanaka, Y., Agarwal, S.K., Ihara, H.: J. Low Temp. Phys. **117**, 903 (1999)
11. Kito, H., Iyo, A., Hirai, M., Crisan, A., Tokumoto, M., Okayasu, S., Sasase, M., Ihara, H.: Physica C **378–381**, 329 (2002)
12. Badica, P., Ihara, H., Iyo, A., Crisan, A.: Supercond. Sci. Technol. **15**, 975 (2002)
13. Liu, R.S., Wu, S.F., Shy, D.S., Tai, C.H., Fu, S.F., Jefferson, D.A.: Chin. J. Phys. **31**, 951 (1993)
14. Bardeen, J., Cooper, L.N., Schrieffer, J.R.: Phys. Rev. B **108**, 1175 (1957)
15. Ihara, H., Iyo, A., Tanaka, K., Tokiwa, K., Ishida, K., Terada, N., Tokumoto, M., Sekita, Y., Tsukamoto, T., Watanabe, T., Umeda, M.: Physica C **282–287**, 1973 (1997)
16. Nawazish, A.K., Khurram, A.A.: Appl. Phys. Lett. **86**, 152502 (2005)
17. Nawazish, A.K., Hussnain, G.: Physica C **436**, 51–58 (2006)
18. Salamati, H., Kameli, P.: Physica C **403**, 60–66 (2004)
19. Kulkarni, A.D., de Welte, F.W., Prade, J., Schroder, U., Kress, W.: Phys. Rev. B **41**, 6409 (1990)